Radboud University Nijmegen

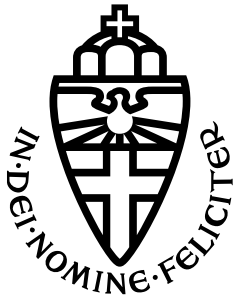

Faculty of Science

Modelling the muon anomalous magnetic moment with non-unified sfermion masses

Exploring the possibility of split masses in the Minimal Supersymmetric Standard Model

Bachelor Thesis Physics & Astronomy

Author:
Jelle Staals

Supervisors:
prof. dr. W.J.P. Beenakker
& J.W. Kip MSc

Second reader:
prof. dr. C.W.J.P. Timmermans

June 2022

Contents

1 Introduction

The Standard Model (SM) incorporates three of the four fundamental forces, i.e. the strong, weak and electromagnetic forces, and is the best theory physics has to explain the universe around us. The SM is a model of elementary particles and their properties and interactions from which we can describe the universe. One of these properties is the magnetic moment of particles that arises from the spin and interactions with the photon. The muon is a particle with spin and interactions with photons and thus has a magnetic moment. Without quantum corrections we would expect the spin magnetic moment of the muon to be a factor 2 larger than the classical orbital magnetic moment of the muon. Once quantum corrections are applied this factor is not exactly 2 anymore. The deviation from the factor 2 indicated by g-2 is called the anomalous magnetic moment. This anomalous magnetic moment is the only significant deviation between the SM and experimental findings at present.

In 2001 the Brookhaven National Laboratory released their measurement of the muon anomalous magnetic moment stating a discrepancy of $3,3\sigma$ between the experimental value and the theoretical prediction. Later in 2021 the Fermi National Accelerator Laboratory released their measurement for the experimental anomalous magnetic moment of the muon. The discrepancy between the experimental and theoretical value is now $4,2\sigma$. The experimental and theoretical values as of the writing of this thesis:

$$a_\mu^{exp} = 116592061(41) \times 10^{-11} \tag{1.1}$$

$$a_\mu^{SM} = 116591810(43) \times 10^{-11} \tag{1.2}$$

It seems that the smaller the uncertainty of the experimental value and the smaller the uncertainty of the theoretical SM prediction, the more significant the difference between the two values becomes.

The threshold for new physics is 5σ. A deviation of $4,2\sigma$ is therefore very close to being a discovery. It is hence important to start developing physics beyond the SM (BSM) that might be able to explain the deviation. One of the most promising BSM theories is the theory of supersymmetry (SUSY). In this thesis we will be looking at a supersymmetric extension of the SM and vary its parameters to determine if our specific implementation of SUSY is a viable extension on the SM that can explain the difference between the experimental and theoretical values.

We are going to use the minimal supersymmetric standard model (MSSM) with minimal supergravity (mSUGRA) unification and non-minimal SUGRA unification to calculate the contributions these models can add to the theoretical value for the muon anomalous magnetic moment. The non-minimal SUGRA model will treat supersymmetric partners of left-handed particles differently from supersymmetric partners of right-handed particles. We will be using SPheno to calculate the particle spectra and g-2 for both models. We will then discuss if treating "handedness" of the particles differently will result in better predictions of the anomalous magnetic moment.

In section 1 we will go over the theoretical background of the magnetic moment and the origin of the anomalous magnetic moment. We will then shortly explain the SM and its properties that give us the theoretical value of the muon anomalous magnetic moment. In section 2 we will explain the concept of SUSY and the contributions it can make to the anomalous magnetic moment. We will then introduce the models used to determine g-2 and the key differences between them. In section 3 the computational programs used will be explained as well as the parameter values. The results are shown and analysed in section 4. In this entire thesis we will use natural units such that $c = \hbar = 1$.

2 Magnetic moment

2.1 Classical mechanics

To understand what the g-factor represents we first need to discuss the origin of the magnetic moment. This can be done in two different ways: the classical approach via electrodynamics and the quantum mechanical approach using the concept of spin and photon interaction.

The magnetic moment is the result of a current inside a system. When exposed to an external magnetic field, the magnetic moment will create a torque to align the system with the external magnetic field, thereby resulting in a precession. The magnetic dipole moment $\vec{\mu}$ is defined by:

$$\vec{\mu} \equiv \frac{1}{2}\int_V \vec{r} \times \vec{J}\, dV = \frac{1}{2}\int_V \vec{r} \times (\rho_q \vec{v})\, dV, \tag{2.1}$$

where V is the volume over which we integrate, $\vec{r}$ the position vector and $\vec{J}$ the current density inside the volume [1]. $\vec{J}$ can be written as the density of charge ρ_q times the velocity $\vec{v}$ of the charge.
If we replace the current density with some loop of current I enclosing an area A, the resulting magnetic dipole moment can be described by:

$$\vec{\mu} = IA\, \vec{u}_{\vec{r}\times\vec{J}}\,,$$

where $\vec{u}_{\vec{r}\times\vec{J}}$ is the unit vector normal to the area A [2]. In figure (2.1) such a loop with magnetic moment is illustrated.
We can now relate the magnetic moment with orbital angular momentum $\vec{L}$ defined by:

$$\vec{L} = m(\vec{r} \times \vec{v}) = \iiint_V \vec{r} \times (\rho\vec{v})\, dV,$$

so that combining it with equation (2.1) gives us:

$$\vec{\mu} = \frac{q}{2m}\vec{L} = g_l \frac{q}{2m}\vec{L}\,, \tag{2.2}$$

where q is the total charge of the system and m is the mass of the system which for large numbers of particles can be written as the mass density ρ times the volume V. The dimensionless quantity g is called the g-factor and for the classical case the g-factor is equal to $g_l = 1$.

The work done by the disk due to the magnetic moment results in a change in potential energy. If we call θ the angle of misalignment between the normal vector $\vec{u}_{\vec{r}\times\vec{J}}$ and the magnetic field $\vec{B}$, we can now express the potential energy U in terms of $\vec{\mu}$, $\vec{B}$ and θ[3]:

$$U = \int \vec{\tau} \cdot d\vec{\theta} = \int (\vec{\mu} \times \vec{B}) \cdot d\vec{\theta} = \mu B \int sin(\theta) d\theta = -\vec{\mu} \cdot \vec{B}\,, \tag{2.3}$$

where the integration is done with respect to an arbitrary reference point. In figure (2.2) it is shown how a torque is generated by the magnetic moment of a disk. The disk will keep rotating towards the field lines of the magnetic field till the magnetic moment is parallel or anti-parallel with the direction of the magnetic field. The disk will always rotate towards the direction that decreases the misalignment angle. A misalignment angle of 0 means there is no work done and the disk will not rotate anymore.

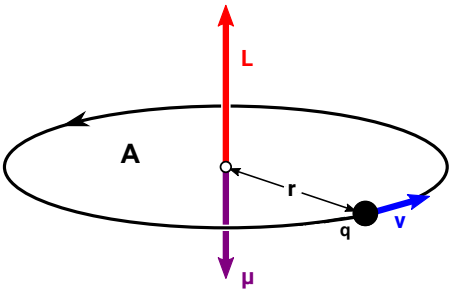

Figure 2.1: Circular motion of a negative charge q enclosing an area A at distance r, with a velocity $\vec{v}$. The resulting current creates a magnetic moment $\vec{\mu}$ and angular momentum $\vec{L}$ perpendicular to the surface. Source: MikeRun [4]

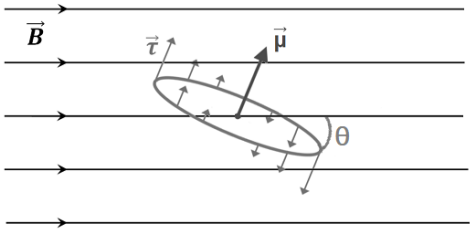

Figure 2.2: Torque $\vec{\tau}$ created by the magnetic moment $\vec{\mu}$ with misalignment angle θ between the disk and magnetic field $\vec{B}$. Source: S. Zurek [5]

2.2 Quantum mechanics

To find the g-factor in quantum mechanics we have to look at wave functions that govern the states of particles. The Schrödinger equation is a linear partial differential equation that represents the time evolution of a physical system in quantum mechanics. The general time-dependent equation is given by:

$$i\hbar\frac{\partial}{\partial t}\Psi(t) = \hat{H}\Psi(t) \,,$$

where $|\Psi(t)\rangle$ is the state vector. The Schrödinger–Pauli equation is a modification of the Schrödinger equation that includes the interactions of a spin-1/2 particle with an external electromagnetic field. For a spin-1/2 particle with mass m and charge q in a static electromagnetic field the Schrödinger–Pauli equation is [6]:

$$i\hbar\frac{\partial}{\partial t}|\Psi\rangle = \left[\frac{1}{2m}\left[(\hat{\vec{p}} - q\vec{A})^2 - q\hbar\vec{\sigma}\cdot\vec{B}\right] + q\psi\right]|\Psi\rangle \,, \tag{2.4}$$

where $\hat{\vec{p}} = -i\hbar\nabla$ is the momentum operator in position space, ψ the electric scalar potential, $\vec{A}$ the magnetic vector potential and $\vec{\sigma} = (\sigma_x, \sigma_y, \sigma_z)$ a vector representation of the Pauli matrices. This Schrödinger–Pauli equation is the non-relativistic limit of the Dirac equation including EM interactions, so that all relativistic effect are neglected. We are looking for the effects of a magnetic field on a particle and in equation (2.4) this effect is nicely isolated with only some constants and the inner product between the Pauli matrices and the magnetic field. This term has a similar shape as equation (2.3) and since the Pauli matrices can be written in terms of the spin angular momentum operator $\hat{\vec{S}}$ as:

$$\hat{\vec{S}} = \frac{\hbar}{2}\vec{\sigma} \,,$$

we can construct an intrinsic magnetic moment such that:

$$\vec{\mu_s} = \frac{q\hbar}{2m}\frac{2}{\hbar}\vec{S} = \frac{q}{m}\vec{S} \tag{2.5}$$

If we take equation (2.2) and (2.5) we get the total magnetic moment:

$$\vec{\mu}_{tot} = \vec{\mu_l} + \vec{\mu_s} = \frac{q}{2m}\left(g_l\vec{L} + g_s\vec{S}\right) \ . \tag{2.6}$$

We already have $g_l = 1$ and can now see from equations (2.5) and (2.6) that $g_s = 2$. This value for g_s is the simplest interaction between the magnetic field and the particle. Interactions involving virtual particles cause deviations to the dimensionless magnetic moment g_s. We are only interested in the deviations to g_s so we can define the anomalous magnetic moment a as:

$$a_l \equiv \frac{g_s - 2}{2}$$

Here the l denotes the lepton we are interested in, e.g., a_μ for the muon anomalous magnetic moment.

2.3 Muon g-2 experiment

To be able to use the anomalous magnetic moment as an indicator of BSM physics we need to know both the theoretical and experimental values and their uncertainties for a_l. Since the contributions to a_l can be approximated as proportional to m_l^2/Λ_{NP}^2, where Λ_{NP} is the mass scale of the "New Physics" model (NP) or BSM physics. We can see that the larger the mass of the lepton the bigger the contribution to a_l [7]. This makes the tau lepton a priori the best candidate to measure the effect of NP. However the tau lepton is too short lived, making it hard to precisely measure the experimental value of a_τ. The next best option is the muon lepton with a $(m_\mu/m_e)^2 \sim 4,2 \cdot 10^4$ relative increase of the sensitivity to NP contributions to g-2 as compared to the electron. To get the theoretical value one needs to keep adding higher orders for smaller uncertainties, but the experimental value by definition has all higher-order corrections embedded. By decreasing the statistical and systematic uncertainties of the experimental value, the discrepancy can be more visible and if the experimental anomalous magnetic moment exceeds the SM prediction by more than 5σ, it can be considered a discovery.

In 2017 Fermilab started the E989 (Muon g-2) experiment, which uses the same muon storage ring and magnet as in the earlier E821 muon g-2 experiment conducted at Brookhaven National Laboratory (BNL), but has a better injection method and longer running time to reduce the uncertainty to four times smaller than observed by BNL. The E821 magnet creates a highly uniform magnetic field in the muon storage ring which is very precisely known. The antimuons used in the E989 experiment get injected as a beam into the storage ring. These antimuons have the same anomalous magnetic moment as muons.
As shown before, a magnetic moment creates a torque. Because the antimuons travel in a circle and inside a uniform magnetic field, the torque in turn creates a precession. Because antimuons decay into neutrinos and positrons, we can measure the amount of positrons detected as a function of time to measure the precession of the antimuon before decay. Longer running time increases the precision of the measurements, thus reducing the uncertainty. The frequency of the precession caused by the magnetic moment is the difference between the spin precession and the relativistic cyclotron precession of the antimuon. The relativistic cyclotron precession is along the magnetic field and does not change over time, meaning it stays in the direct of $\vec{B}$. The resulting frequency is given by [8]:

$$\vec{\omega_a} = -\frac{g-2}{2}\frac{q\vec{B}}{m_\mu} = -a_\mu\frac{q\vec{B}}{m_\mu} \tag{2.7}$$

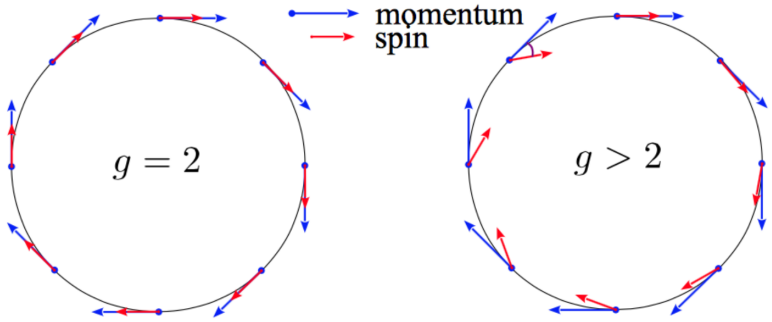

Figure 2.3: Muons travelling in a circular ring with the momentum vector in blue and the spin vector in red. On the left there is no misalignment for $g = 2$. Once the g-factor is larger than 2 the misalignment after one rotation is measurable as shown on the right. Source: E. Valetov [11]

It is clear that for $g = 2$ the frequency will vanish. Because the cyclotron frequency does not deviate from the direction of the magnetic field we can see that the misalignment of the spin precession results in a non-zero $\vec{\omega_a}$. This is schematically represented in figure (2.3).

On April 7, 2021 Fermilab National Accelerator Laboratory (FNAL) released the first results for the experiment. The measured muon anomalous magnetic moment is:

$$a_\mu^{FNAL} = 116592040(54) \times 10^{-11} \ ,$$

with the uncertainty of the last two digits in parentheses. This agrees with the BNL E821 result and corresponds to $3,3\sigma$ difference with the SM prediction.

Combining the FNAL E989 result with the BNL E821 result we find the combined experimental average and theoretical SM prediction to be [9][10]:

$$a_\mu^{exp} = 116592061(41) \times 10^{-11} \tag{2.8}$$

$$a_\mu^{SM} = 116591810(43) \times 10^{-11} \tag{2.9}$$

The difference, $\Delta a_\mu = a_\mu^{exp} - a_\mu^{SM} = (251 \pm 59) \times 10^{-11}$, has a significance of $4,2\sigma$.

2.4 The Standard Model and contributions to a_μ

The SM is a theory that contains all known elementary particles and describes three of the four fundamental forces in the universe. The fundamental forces integrated in the SM are the electromagnetic, the weak and the strong force. It is the most accurately tested theory to date in particle physics. The elementary particles can be categorised into fermions governed by Fermi-Dirac statistics and bosons governed by Bose-Einstein statistics. The interactions of elementary particles are described by a gauge theory where the gauge bosons act as mediators of the interactions between fermions.

Fermions are half-integer spin particles and are the basic building blocks of matter. There are twelve fermion types: six leptons and six quarks. The leptons and quarks can be further subdivided into three generations or families. The first generation quarks

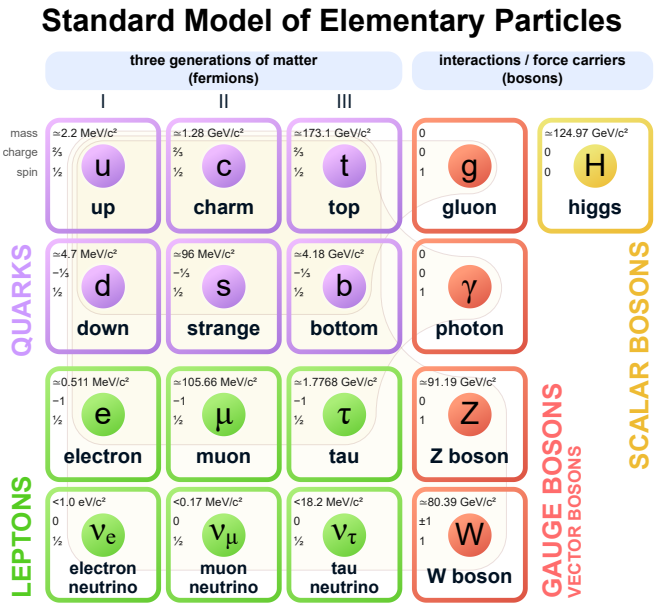

Figure 2.4: The Standard Model of elementary particles: the twelve fermions and five bosons. The fermions shown in purple and green split into the quarks and the leptons respectively. The bosons shown in red and yellow split into vector bosons and the scalar Higgs boson respectively. Source: PBS NOVA [12]

are the up and down quarks. The second generation quarks are the charm and strange quarks and the third generation consists of the top and bottom quarks. For the leptons we have the first generation electron and electron neutrino, the second generation muon and muon neutrino and the third generation tau and tau neutrino. All fermions have an associated antiparticle with opposite charge and lepton/baryon number.

Bosons are integer-spin particles and are known as the force carriers that mediate interactions. The bosons can be categorised into different spins. The bosons with a spin of 1 are called gauge/vector bosons. The known gauge bosons are the photon, $W^{\pm}$ and Z boson, and the gluons. The boson with a spin of 0 is called the (scalar) Higgs boson and is responsible for giving mass to the fermions and the $W^{\pm}$ and Z bosons via the Higgs mechanism. All bosons are their own antiparticle except for the W boson that changes sign, W^{+} is the anti particle of W^{-} and vice versa. All elementary particles with their mass, charge and spin are shown in figure (2.4).

The Higgs mechanism explains the generation of mass for the $W^{\pm}$ and Z bosons as caused by a property of the Higgs potential. The Higgs potential has a minimum with a non-zero vacuum expectation value (vev). This vev permeates all of spacetime and the coupling to this vev gives mass to the bosons. The combination of the electromagnetic interactions and weak interactions is called the electroweak (EW) sector. This EW interaction has a $SU(2)_L \otimes U(1)_Y$ symmetry, with L denoting the left-handed chirality and Y denoting the weak hypercharge. Due to the shape of the Higgs potential and the non-zero vev, the EW gauge group has to spontaneously break its symmetry: the gauge symmetry $SU(2)_L \otimes U(1)_Y$ breaks to $U(1)_{EM}$.

This results into the generation of mass for the previously massless bosons, the $W^{\pm}$ and Z bosons are created. Since the gauge symmetry $U(1)_{EM}$ is left unbroken the boson related to this symmetry, the photon, does not acquire a mass.

The SM contributions to the anomalous magnetic moment can now be split into three parts [13]:

$$a_\mu^{SM} = a_\mu^{QED} + a_\mu^{EW} + a_\mu^{Hadron} \tag{2.10}$$

The QED (quantum electrodynamic) term includes all photonic and leptonic (e, μ, τ) loops represented in Feynman diagrams. The EW term includes all loops involving the heavy $W^{\pm}$, Z or Higgs particles. The last term incorporates all hadronic (quark and gluon) loop contributions to a_μ, related to the $SU(3)_C$ gauge group with C denoting the colour charge of quarks and gluons.

2.4.1 Quantum electrodynamic contribution

The dominant contributions to the muon anomalous magnetic moment come from the QED corrections, with the one loop contribution as the largest correction to a_μ. This contribution is due to fluctuations arising from muon-photon interactions and was proposed by Schwinger in the 1940's. For the one loop contribution we get a correction to the g-factor of [14]:

$$a_\mu^{QED} = \frac{\alpha}{2\pi} \, ,$$

with the fine-structure constant $\alpha = e^2/(4\pi\epsilon_0\hbar c)$.
To find the higher loop-level contributions we can write a_μ^{QED} into a more general form:

$$a_\mu^{QED} = A_1 + A_2\left(\frac{m_\mu}{m_e}\right) + A_2\left(\frac{m_\mu}{m_\tau}\right) + A_3\left(\frac{m_\mu}{m_e}, \frac{m_\mu}{m_\tau}\right) \, , \tag{2.11}$$

where m_e, m_μ and m_τ are the masses of the electron, muon and tau, respectively. The term A_1 contains only photons and muons and is independent of electron and tau mass. The terms A_2 and A_3 are functions of the mass ratios m_μ/m_e and m_μ/m_τ and are generated in diagrams containing electrons and taus. Each of the A_i ($i = 1, 2, 3$) in equation(2.11) can be expanded as an infinite power series in α/π [15]:

$$A_i = A_i^{(2)}\left(\frac{\alpha}{\pi}\right) + A_i^{(4)}\left(\frac{\alpha}{\pi}\right)^2 + A_i^{(6)}\left(\frac{\alpha}{\pi}\right)^3 + A_i^{(8)}\left(\frac{\alpha}{\pi}\right)^4 + \dots \, .$$

An n-loop Feynman diagram can be seen in the $2n$th-order of the perturbation series of QED. For every additional loop the number of vertices is increased by 2. We can now see that the one loop contribution is the evaluation of the lowest order contribution: $A_1 = 1/2$ and $A_2 = A_3 = 0$. This can also be seen in figure (2.5). In figure (2.6) all two loop Feynman diagrams that contribute to $g - 2$ are shown. As of 2022 all contributions up to the three-loop QED corrections are known analytically. For the four-loop corrections more than a thousand Feynman diagrams are needed to evaluate the contribution to a_μ^{QED} and only a few of those are known analytically. The rest is computed numerically.

Summing the known terms in the perturbative QED expansion, we obtain the following QED contribution to the muon anomalous magnetic moment [10][16]:

$$a_\mu^{QED} = 116584718.931(104) \times 10^{-11} \, , \tag{2.12}$$

where the uncertainty is a sum of uncertainties due to the uncertainty on the tau mass, the fine-structure constant α and higher-order QED in order of increasing errors respectively.

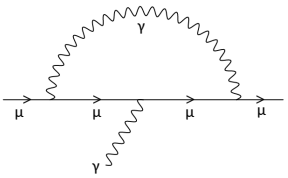

Figure 2.5: The Feynman diagram at one-loop. There is only one one-loop diagram. The straight and wavy lines represent lepton and photon propagators respectively.

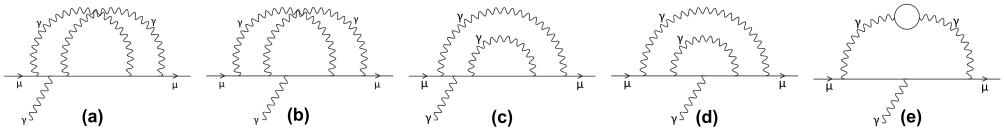

Figure 2.6: The Feynman diagram at two-loop. There are seven distinctly different two-loop diagrams. The time-reversed diagrams for (a) and (c) are not shown. Furthermore (e) has a vacuum polarization containing short-lived virtual particle–antiparticle pairs. The straight and wavy lines represent lepton and photon propagators respectively.

2.4.2 Electroweak and Hadronic contributions

The EW contribution is a combination of all contributions made by the $W^{\pm}$, Z and H bosons. The EW one-loop contribution is given by[17]:

$$a_{\mu}^{EW(1)} = \frac{G_F}{\sqrt{2}} \frac{m_{\mu}^2}{8\pi^2} \left[\frac{5}{3} + \frac{1}{3}(1 - 4s_W^2)^2 \right] = 194.79(1) \times 10^{-11} \,,$$

where G_F is the Fermi constant and $s_W^2 = (1 - m_W^2/m_Z^2) = \sin^2(\theta_W)$ involves the weak mixing angle θ_W and is defined by the masses of $W^{\pm}$ and Z bosons. Because the contribution is proportional to the inverse of the masses we can see that the Z and H boson are more suppressed in the contributions than the $W^{\pm}$ boson. We can write the contribution in a different way:

$$a_{\mu}^{EW(1)} \propto \frac{\alpha}{4\pi s_W^2} \frac{m_{\mu}^2}{m_W^2}$$

We now see that the contribution gets suppressed by the small mass ratio $m_{\mu}^2/m_W^2 \approx 10^{-6}$. If we write the total computed EW contribution as a sum of all n-loop contributions we see that the one-loop contribution is by far the largest contribution. The contribution of the electroweak interaction is [13]:

$$a_{\mu}^{EW} = a_{\mu}^{EW(1)} + a_{\mu}^{EW(2)} + a_{\mu}^{EW(\geq 3)} = 153.6(1.0) \times 10^{-11} \tag{2.13}$$

Here the $a_{\mu}^{EW(\geq 3)}$ term indicates all diagrams with three or more loops that have been computed.

The hadronic contributions are complicated to calculate and give rise to the biggest uncertainty of the theoretical prediction. The contribution is described by quantum chromodynamics (QCD) and cannot be calculated using conventional computational methods. In figure (2.7) the one loop diagrams for the EW and hadronic contributions are shown.

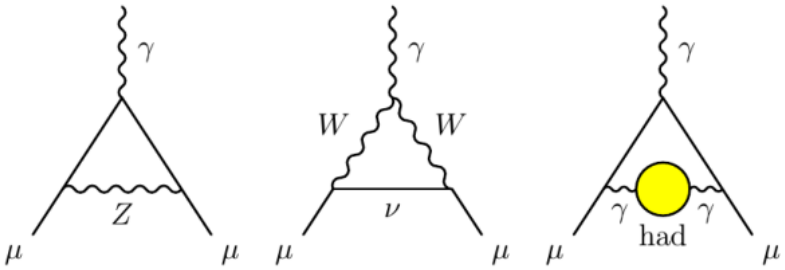

Figure 2.7: A one loop Feynman diagram with electroweak Z-boson exchange (left), electroweak W-boson exchange (middle) and hadronic vacuum polarization exchange (right). Source: Cern [19]

The hadronic contributions can be split in the hadronic vacuum polarization (HVP) and hadronic light-by-light (HLbL) contributions. With experimental measurements the hadronic contribution is determined to be [18]:

$$\begin{aligned} a_\mu^{Hadronic} &= a_\mu^{HVP} + a_\mu^{HLbL} \\ &= 6845(40) \times 10^{-11} + 92(18) \times 10^{-11} \\ &= 6937(43) \times 10^{-11} \end{aligned} \tag{2.14}$$

If we know fill in equations (2.12), (2.13) and (2.14) in (2.10) we get the result for the SM prediction given in equation (2.9).

3 Supersymmetry

As shown above the difference between the observational and theoretical muon anomalous magnetic moment is $4,2\sigma$. If observation and theory differ by 5σ we call it a discovery and new physics is needed to explain the difference. Although the deviation is not yet 5σ, a fairly robust hint towards sew physics is present. Including BSM physics could match the theoretical prediction to the experimental observations of a_μ.

There are many BSM theories that are an extension of the SM and one of the most prominent theories is SUSY. SUSY can solve multiple problems at the same time due to its introduction of new particles and concomitant parameters. The principle is straightforward, each fermion has a bosonic superpartner (sfermion) and every boson has a fermionic superpartner (bosino). This would make the theory symmetric regarding fermions and bosons, solving certain problems with the SM. The SUSY theory that will be discussed and used in the modelling and plotting will be a constraint variation of the Minimal Supersymmetric Standard Model (MSSM). The new supersymmetric particles (sparticles) that are important in this thesis are shown in table (3.1).

Sparticle	Superpartner	Description
Sfermion	Charged slepton ($\tilde{\ell}^{\pm}$)	The superpartners of the charged leptons (electron, muon, tau). The charged sleptons are labelled from lightest to heaviest: $\tilde{\ell}_1^{\pm}$, $\tilde{\ell}_2^{\pm}$, $\tilde{\ell}_3^{\pm}$.
	Sneutrino ($\tilde{\nu}_L$)	The superpartners of the neutrinos. There are only left-handed sneutrinos. The sneutrinos are labelled from lightest to heaviest: $\tilde{\nu}_1$, $\tilde{\nu}_2$, $\tilde{\nu}_3$.
Bosino	Chargino ($\tilde{\chi}^{\pm}$)	The superposition of the superpartners of the Higgs boson and W boson. The charginos are labelled from lightest to heaviest: $\tilde{\chi}_1^{\pm}$, $\tilde{\chi}_2^{\pm}$.
	Neutralino ($\tilde{\chi}^0$)	The superposition of the superpartners of the Higgs boson, Z boson and photon. The neutralinos are labelled from lightest to heaviest: $\tilde{\chi}_1^0$, $\tilde{\chi}_2^0$, $\tilde{\chi}_3^0$, $\tilde{\chi}_4^0$.

Table 3.1: The added sparticles of the MSSM and their descriptions.

3.1 Problems with the Standard Model

One problem of the SM is that it does not include gravity, which means at some high energy scale new physics takes over to account for gravity. The consequence of this is the accumulation of mass by the Higgs boson due to quantum corrections. This creates a new problem: the Higgs boson mass has been measured to be around 125 GeV, while the predicted Higgs boson mass due to BSM physics has to be at least an order of magnitude higher. To solve this problem, it is thus needed for the BSM theory to incorporate a mechanism that counters the large corrections on the Higgs boson mass. SUSY protects the Higgs boson mass from large corrections via counter terms that cancel out the corrections.

Another interesting consequence of SUSY is the possibility of unification of the three coupling constants, which is not present in the SM. If we plot the strength of the fundamental forces against energy for only the SM we see the forces nearly intersecting in a single point at very high energies, as shown in figure (3.1). This could be an indication of BSM physics. SUSY naturally unifies the forces at high energy, making it a very strong argument that SUSY is the right extension of the SM.

Besides the difference in spin between particles and their sparticles, the SM particle and its superpartner have another property that differs called R-parity. In SUSY the lepton and baryon numbers do not have to be conserved. R-parity is a property that ensures that protons cannot quickly decay to lighter particles by exchanging sparticles. The R-parity of particles is $+1$, while sparticles have an R-parity of -1. In the MSSM R-parity is required to be conserved, hence in any decay of a SUSY particle one sparticle needs to remain. If R-parity is preserved a lightest supersymmetric particle (LSP) exists that does not decay. This LSP is therefore a strong dark matter candidate. Because dark matter candidates should be neutral and only interact through weak interactions and gravity, it is clear that the best candidate of dark matter in the MSSM is the neutralino. SUSY could thus be a good extension explaining the light Higgs mass, Grand Unification and dark matter.

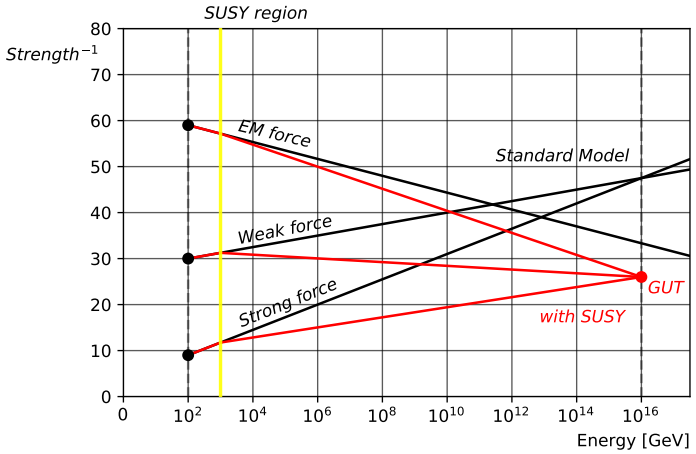

Figure 3.1: The strength of the three fundamental forces incorporated in the Standard model as a function of energy. The red lines unify in a single point at the GUT energy scale due to SUSY. The yellow line indicates the energy scale at which SUSY starts to take effect.

3.2 MSSM

The symmetry that SUSY introduced predicts that the masses of the sparticles are equal to the masses of the SM partner particles. Because the masses of the SM particles are known and can be measured using colliders, we would have been able to measure and find theses sparticles. This is not the case, which means that at some scale between the GUT energy and the energy of SM particles the symmetry has to break. This soft symmetry breaking can be described using the soft SUSY breaking Lagrangian, one of the main parts of the MSSM Lagrangian.

The MSSM is a model that realises SUSY as an extension to the SM and uses the minimal number of parameters consistent with experimental findings [20]. Even though the model uses the minimal number of parameters, due to the unknown mechanisms for symmetry breaking at lower energies the MSSM has 105 free parameters. Since we will be looking at SUGRA as breaking mechanism not all 105 parameters are needed. This constrains the available low-energy parameter space, since it will constrain the individual masses of the sparticles. We cannot freely choose the masses of the sparticles.

3.2.1 mSUGRA

A lot of theories were created to explain the phenomenon of soft-SUSY breaking that produces the desired sparticles with masses above 100 GeV. One of the most researched model explaining soft symmetry breaking is the minimal supergravity model (mSUGRA). This model uses the basis of MSSM, but only needs 4 free parameters and a sign to predict the masses of the sparticles. The model uses a method where SUSY breaking is communicated through gravitational interactions called supergravity [21]. We won't explain this model in detail in this thesis.

The set of parameters needed in mSUGRA are summarised in table (3.2). We can use these parameters to predict the masses of the sparticles using the mSUGRA model and compute the contribution to a_μ. The parameters are input values at the unification energy scale.

Symbol	Description
m_0	The universal scalar mass at GUT energy scale
$m_{1/2}$	The universal gaugino and higgsino mass at GUT energy scale
A_0	The universal trilinear coupling
$tan(\beta)$	The ratio of the vacuum expectation values of the two Higgs doublets
$sign(\mu)$	The sign of the Higgs/higgsino mass parameter

Table 3.2: The free parameters and sign of mSUGRA.

3.2.2 Non-unified SUGRA

The weak interaction is the only interaction of the four fundamental interactions that violates the parity-symmetry. This results in the weak interaction acting only on left-handed particles and right-handed antiparticles. In the m_0 parameter the left-handed and right-handed sparticles have equal mass and are treated equally. We now propose that left-handed and right-handed sparticles have different masses, splitting m_0 into two new free parameters. This splitting might give a bigger contribution to the anomalous magnetic moment, since the left-handed sparticles get treated differently by the weak force than the right-handed sparticles. The splitting of the m_0 parameter gives us:

$$m_0 = \begin{cases} m_{0L} & \text{, for left-handed sparticles} \\ m_{0R} & \text{, for right-handed sparticles} \\ m_{0H} = \sqrt{m_{0L} \cdot m_{0R}} & \text{, geometric average of } m_{0L} \text{ and } m_{0R} \end{cases}$$

The left-handed and right-handed m_0 only affect the sfermions because the bosinos have spin-1/2 and thus will come from $m_{1/2}$. The charged sleptons are left-handed and right-handed, while sneutrinos are only left-handed. For the muon this means there is a $\tilde{\mu}_L^{\pm}$ and $\tilde{\mu}_R^{\pm}$, but only the left-handed $\tilde{\nu}_{\mu_L}$. The mass parameter m_{0H} is the geometric average of m_{0L} and m_{0R} and will make sure that the Higgs boson mass will be within the acceptable theoretical bounds, which will be discussed in Section (4.2). Since m_{0H} depends on m_{0L} and m_{0R}, it is not a free parameter. The non-unified model thus has five free parameter and a sign.

3.3 SUSY contributions

If we consider SUSY to be the extension of the SM, then the effects of SUSY on the muon anomalous magnetic moment will also be of importance. Just like how the QED, EW and hadronic contributions were needed to accurately determine the theoretical value of a_μ, we now need to construct the Feynman diagrams of supersymmetric contributions to predict the a_μ value. To find out which first-order diagrams have the biggest contribution we must first briefly look into the propagator of the diagrams.

In the most simple terms a relativistic propagator gives the amplitude of a particle travelling between two spacetime points. Propagators $\Psi(x - x')$ are solutions to the Klein-Gordon equation:

$$\left(\Box_x + m^2\right) \Psi(x - x') = -i\delta(x - x') \,, \tag{3.1}$$

where x and x' are points in spacetime, m the mass of the particle and $\Box_x = \partial^2/\partial t^2 - \nabla^2$ the d'Álembertian operator acting on x. To find $\Psi(x - x')$ we preform a Fourier transform to momentum space and see:

$$\Psi(x - x') = \int \frac{d^4p}{(2\pi)^4} e^{-ip\cdot(x-x')} \Psi(p) \,, \tag{3.2}$$

where $p \cdot (x - x')$ is the 4-vector inner product. Now solving equation (3.1) using (3.2) we can see that the propagator has the form [22]:

$$\begin{aligned} (-p^2 + m^2)\Psi(p) &= -i \\ \Psi(p) &= \frac{i}{p^2 - m^2} \end{aligned} \tag{3.3}$$

We can see that the propagators are inversely proportional to the square of the mass of particles. Lower masses will thus result in a bigger contribution to a_μ.

The only two one-loop Feynman diagrams that have a loop involving sparticles are the chargino and neutralino loops shown in figure (3.2). These diagrams include the sleptons, specifically the smuon, the sneutrinos, specifically the muon sneutrino, and the chargino and neutralino bosinos.

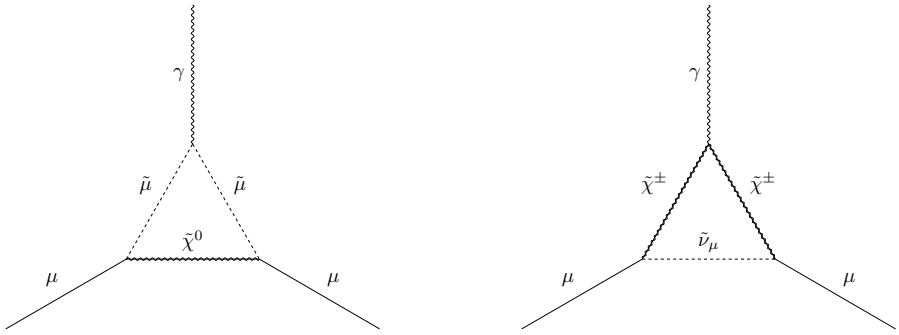

Figure 3.2: All Feynman diagrams with one-loop SUSY contributions. (a) The Feynman diagram involving the neutralino-smuon exchange. (b) The Feynman diagram involving the chargino-sneutrino exchange. Source: D. Stöckinger [23]

4 Computational program

To calculate the contribution of the unified MSSM and the non-unified model to the muon anomalous magnetic moment, the particle spectrum has to be calculated. In the Lagrangian all terms are related to each other and have an influence on the particle spectrum, making it difficult to predict the spectrum given a certain parameter set. Even only considering five parameters will already be too difficult to predict what the particle spectrum will be. Since doing so manually is impractical and unfeasible, computing programs are required

4.1 SARAH

SARAH is a program written in Fortran that provides code for SPheno such that SPheno can compute the particle spectra for a given SUSY model. It creates a model file with input parameters that can be used by spectrum-generator programs like MicrOmegas, WHIZARD and most importantly for us SPheno [24]. SARAH automatically computes the Lagrangian and the evolution of parameters from high to low energy scales, you only need to specify the parameter input values. Since the program does not need the values itself, it will simply compute the relevant equations and necessary files that SPheno needs. It is important to later on select the model points that are important to us, like model points with a good Higgs mass corresponding to the observed value.

SARAH generates template files called Les Houches files for all SUSY models. In table (4.1) the parameter ranges for the five parameters are given. In case of the unified MSSM model the left-handed and right-handed universal scalar mass is equal so that $m_{0L} = m_{0R} = m_0$.

Parameter	Parameter range
m_{0L}	[0,4000]
m_{0R}	[0,4000]
$m_{1/2}$	[0,4000]
A_0	[-4000,4000]
$tan(\beta)$	[1,50]
$sign(\mu)$	$\pm$ 1

Table 4.1: The free parameters and their ranges. All values were chosen at random with a uniform distribution. The sign of μ has an even chance of being positive or negative.

4.2 SPheno

SPheno is short for Supersymmetric Phenomenology and uses the source code generated by SARAH together with experimental data such as the masses of SM particles and their contribution to the anomalous magnetic moment to calculate the SUSY spectrum at energies below the SUSY scale [25]. SPheno can be used for multiple things, but one important feature is the calculation of the Higgs boson mass, which includes two-loop diagrams. In figure (4.1) a visual representation is given of the evolution of high-scale variables to low energies, that is energies below electroweak symmetry breaking (EWSB scale). From the output files of SPheno we can extract the masses of the sparticles as well as the muon anomalous magnetic moment corrections.

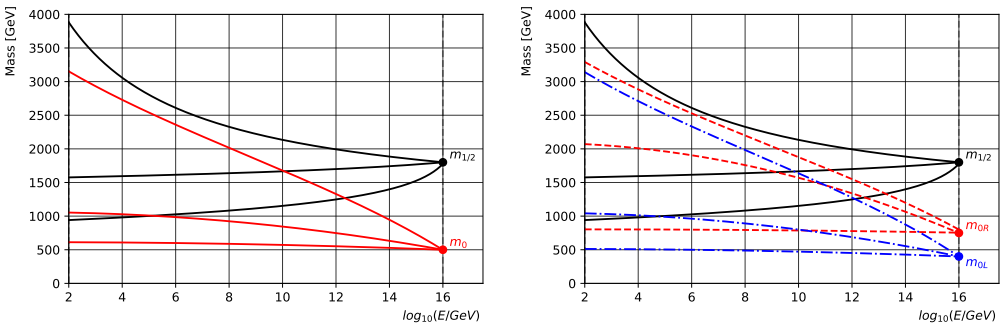

(a) (b)

Figure 4.1: A visual representation of SPheno's spectrum generator for (a) the unified MSSM model and (b) the non-unified model. The spectrum produces the masses of sparticles around the energy scale of 100 GeV, at which we can measure particles in colliders.

Since SPheno simply calculates the values for the sparticle masses and generates the model spectra, all model spectra created by SPheno are valid. However, valid spectra are not by definition good spectra, because theoretical predictions constrain the values for the sparticle masses. To only select the good spectra we add two extra constraints to the models.

The experimental value for the Higgs mass is $125,3(0,6)$ GeV. Because the theoretical SUSY uncertainty of the Higgs mass is larger than the experimental uncertainty, the value of the Higgs mass generated by SPheno has to fall between the values 122 GeV and 128 GeV. SPheno considers a maximum of two-loop corrections to the Higgs mass, while in reality higher-order loop corrections can theoretically cause significant deviations to the Higgs mass and the evolution from high energies adds additional uncertainties.
Since we are also interested in the LSP as a candidate for dark matter, as discussed in Section (3.1), the neutralino needs to be the lightest sparticle. We can disregard spectra that do not conform to these two constraints.

5 Results and Analysis

Using the valid spectra that SPheno calculated we can now look at the contributions of adding SUSY to a_μ. In Section (3.2.1) and (3.2.2) we looked at the free parameters and their importance, where it is expected that m_{0L}, m_{0R} provide the largest impact since we will be changing from a unified m_0 to the non-unified model.

In figure (3.2) we saw the two Feynman diagrams that have the biggest contribution to the muon anomalous magnetic moment. It features the sleptons, sneutrinos, charginos and neutralinos, making these sparticles the most important sparticles to look at. Especially the slepton and sneutrino are of interest due to their relation with m_0, which we split for the non-unified model. We are hence interested in the plots for the slepton and sneutrino mass and their contribution to a_μ as they should show the difference between the unified and non-unified model.

All plots shown below plot the standard unified MSSM and the non-unified model on top of each other. As is shown in figure (5.1) the SUSY contribution to the anomalous magnetic moment is plotted against the mass of the chargino. In this plot the difference between experimental and theoretical muon anomalous magnetic moment Δa_μ is shown in grey with a bandwidth of 2σ. This means that any points inside the grey band have a satisfactory contribution to the anomalous magnetic moment to explain the difference between theory and experiment. It is pretty clear that no model points lie in the grey band. Therefore it is more informative to rescale the y-axis to the region with model points, between $\delta a_\mu = 0$ and $\delta a_\mu = 60 \cdot 10^{-11}$. Furthermore we will only show positive contributions since the plots are symmetric and negative contributions will only decrease a_μ. A total of 20.000 spectra were generated in the first run, with 10.000 spectra for each model. Subsequently for the second run we sampled around points with the largest contribution to a_μ ($\delta a_\mu > 35 \cdot 10^{-11}$) using a normal distribution around the free parameters. After the second run a total of 50.000 spectra, 25.000 for each model, were generated with which the plots below are made. The highest contribution to the muon anomalous magnetic moment is $\delta a_\mu = 63 \cdot 10^{-11}$.

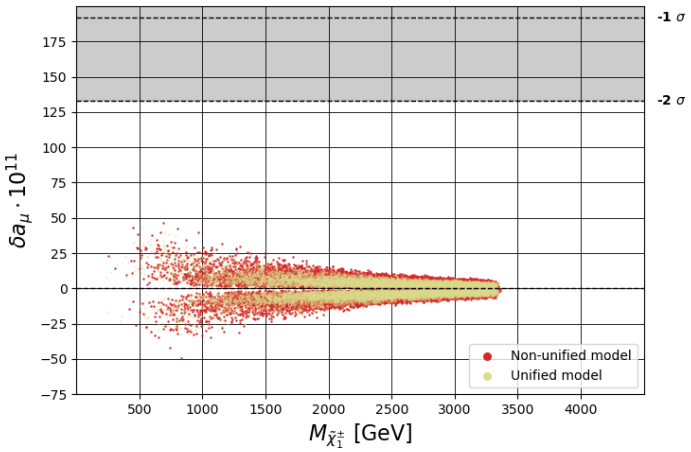

Figure 5.1: The δa_μ dependence on the chargino mass in GeV for the first run. The 1σ and 2σ bands for a_μ are shown in grey.

$\mathbf{m_{0L}}$ vs $\mathbf{m_{0R}}$

The plot depicting the first run distribution of m_{0L} with respect to m_{0R} is shown in figure (5.2). The parameters were scanned uniformly. The distribution looks uniform for all m_{0L} and for $m_{0R} > 500$ GeV. Below 500 GeV we did not find any right-handed m_0 that give valid spectra. In figure (5.3b) it is clear to see that the unified model does not have model points for m_0 below 500 GeV. The left-handed m_0 in the non-unified model can go below 500 GeV due to the asymmetry when regarding the purely left-handed sneutrino.

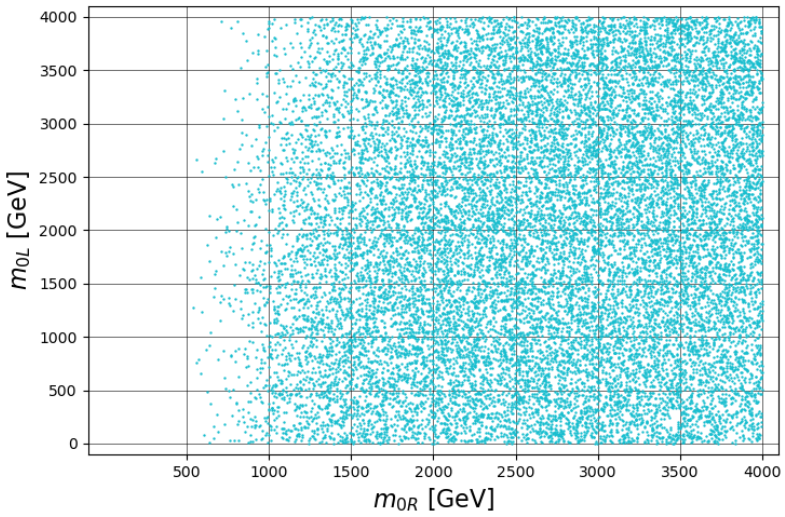

Figure 5.2: The relation between m_{0L} and m_{0R} for the first run. Both masses are sampled uniformly and model points with wrong Higgs masses and lightest neutralino mass that is not LSP are removed.

$\mathbf{m_0}$

In figure (5.3) we can see the dependence of δa_μ on the high-energy mass parameter for sfermions for left- and right-handed sparticles. Just like in figure (5.2) it is clear to see that the left-handed mass term can be lower than the right-handed mass term, most likely due to the asymmetry of left- and right-handed sparticles. We can see that the plots for m_{0L} and m_{0R} look similar but shifted, this can be explained by the geometric average mass m_{0H}. The unified model mass m_0 stays strictly above 500 GeV. Because we are using $m_{0H} = \sqrt{m_{0L}m_{0R}}$ for the non-unified model, the m_{0R} is able to compensate for the low mass of m_{0L}. This is important because we typically need m_0 to be heavy to get the correct Higgs mass. The lower masses for m_{0L} do seem to have some small effect on δa_μ compared to m_0, but not enough to explain the discrepancy in the anomalous magnetic moment. In later plots it will become clear why this dissimilarity in handedness is of significant importance to the contributions.

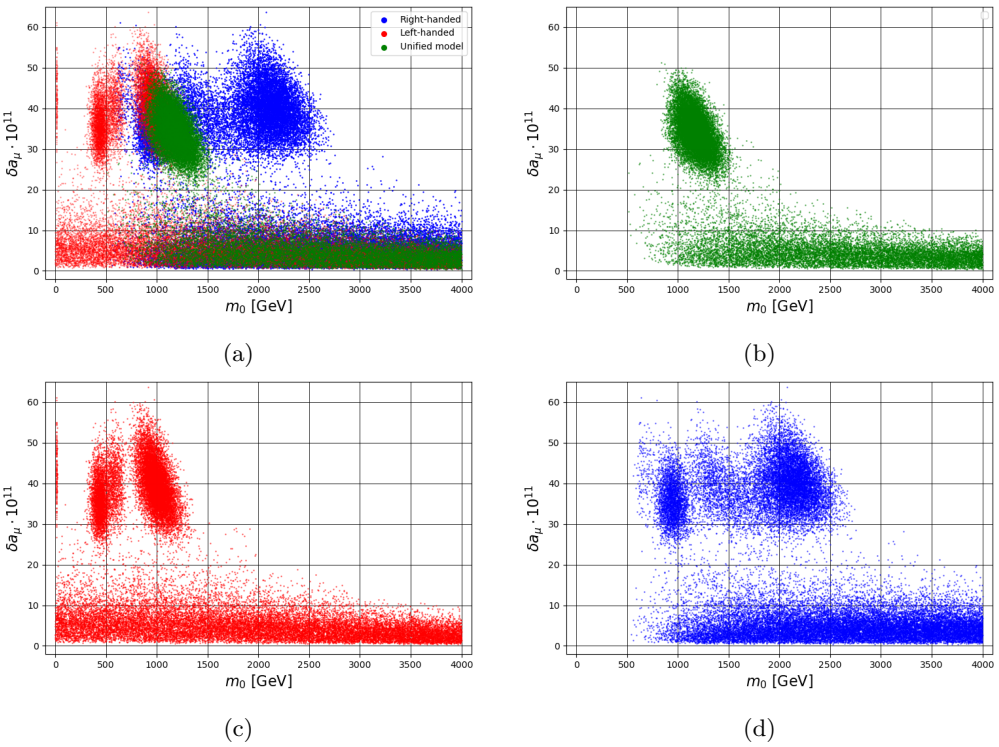

Figure 5.3: The dependence of δa_μ on the universal scalar masses m_0, m_{0L} and m_{0R} in GeV in the unified and non-unified model for all runs.

Slepton mass

In figure (5.4) the dependence of δa_μ on the lightest slepton mass is shown. In purple the non-unified model is shown while the unified model is shown in orange. Immediately one can see the difference between the two models. Namely, the non-unified model has, compared to the unified model, a larger contribution to a_μ. We can see that for lower slepton masses both models show better results, which is to be expected due to the m^{-2} relation between the contribution to a_μ and the mass of sparticles given in equation (3.3). We can observe the plot points of the second run located below a mass of 1500 GeV and around $\delta a_\mu = 40 \cdot 10^{-11}$. These points correspond to fairly low values of m_{0L} and m_{0R}. Because we have taken a normal distribution around the points with high contributions for the second run, the clustering is simply a scanning artefact.

Figure (5.5) shows the same x- and y-axis as in figure (5.4), but with a logarithmic y-axis. This allows us to see the σ bands and how far the models are from these bands. It might be possible to reach the 2σ band around Δa_μ if the slepton mass is sufficiently small, but this might be impossible due to multiple restrictions on the mass of the slepton, such as the limitations that it has to be higher than the neutralino mass. Due to our choice of symmetry breaking the Higgs boson mass also drives up the mass of the slepton, making it harder to get smaller masses for the slepton while still having the correct mass for the Higgs boson

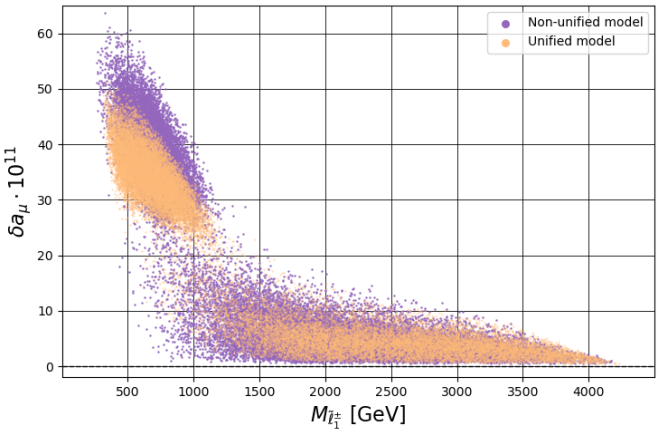

Figure 5.4: The dependence of δa_μ on the lightest slepton mass in GeV in the unified (orange) and non-unified (purple) model for all runs.

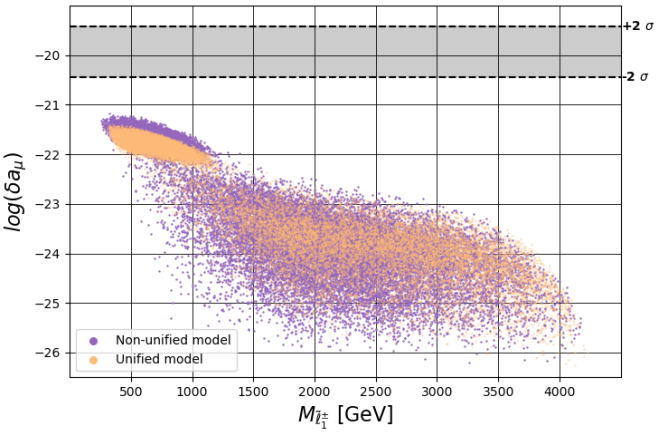

Figure 5.5: The dependence of the logarithm of δa_μ on the lightest slepton mass in GeV in the unified (orange) and non-unified (purple) model for all runs.

Sneutrino mass

The plots depicting the lightest sneutrino mass are shown in figures (5.6) and (5.7). The plots look similar to the plots for the slepton mass, which is to be expected since they follow the same mass relation and their diagrammatic contributions are similar. However, there is a difference between the slepton and sneutrino plots. The non-unified model plot has a significantly smaller sneutrino mass than the unified model plot for the sneutrino. This is due to absence of right-handed sneutrinos. In the plots for the slepton mass, the model points of the two models were on top of each other, this is not the case with the sneutrino. The model points of the non-unified model are not on top of the model points of the unified model, instead model points of the second run of the non-unified model have lower masses than model points of the unified model. This shift shows the impact of splitting m_0 more clearly than the plots for the slepton, because there are only left-handed sneutrinos to make contributions to δa_μ.

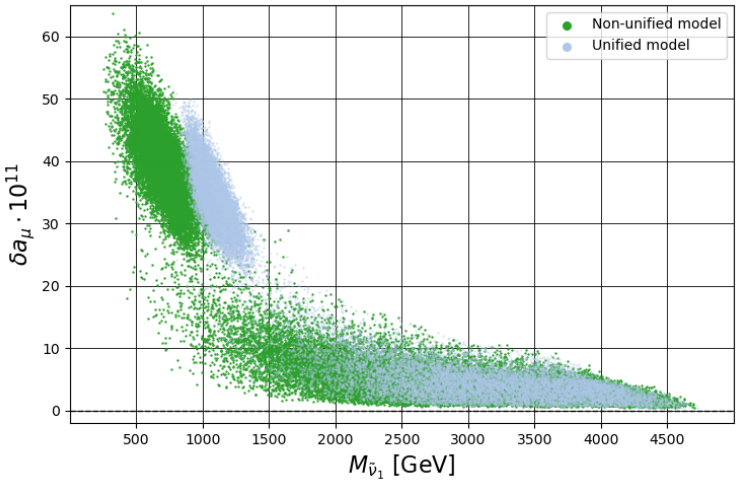

Figure 5.6: The dependence of δa_μ on the lightest sneutrino mass in GeV in the unified (light blue) and non-unified (green) model for all runs.

The logarithmic plot of the sneutrino tells us a similar story as the logarithmic plot of the slepton. The unified model does not go below the 500 GeV threshold because m_0 needs to be sufficiently large, while the non-unified model can have lighter sneutrino masses. As a consequence we can see higher contributions for the non-unified model. Even though the contribution is higher for the non-unified model, it will still be difficult to reach the 2σ band. It might be possible with multiple new runs for the model points with the highest contributions.

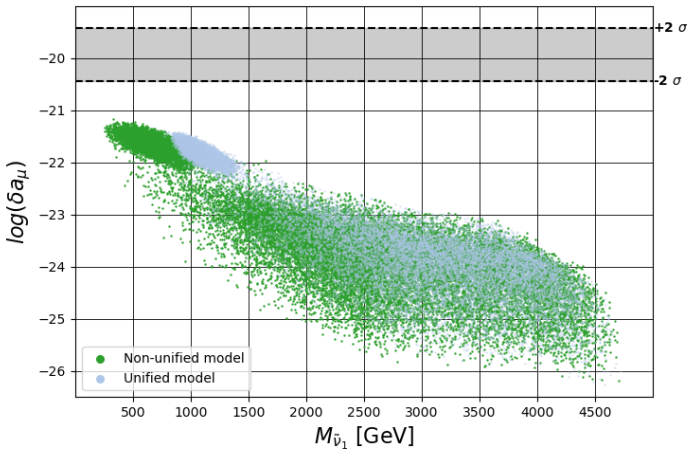

Figure 5.7: The dependence of the logarithm of δa_μ on the lightest sneutrino mass in GeV in the unified (light blue) and non-unified (green) model for all runs.

Chargino mass

In figures (5.8) and (5.9) the relation between δa_μ and the first chargino mass is illustrated. Just like the previous graphs the overall trajectory follows the $M^{-2}_{\tilde{\chi}^\pm_1}$ relation. The chargino unified-model plot looks similar to the slepton and sneutrino plots in figures (5.4) and (5.6) and just like those plots the lowest first chargino mass lies roughly at 500 GeV. The non-unified model plot does look a bit different; it has two clusters of points between $25 \cdot 10^{-11} < \delta a_\mu < 60 \cdot 10^{-11}$. One of the clusters is located at a first chargino mass of 500 GeV, while the other is located around 900 GeV. Because

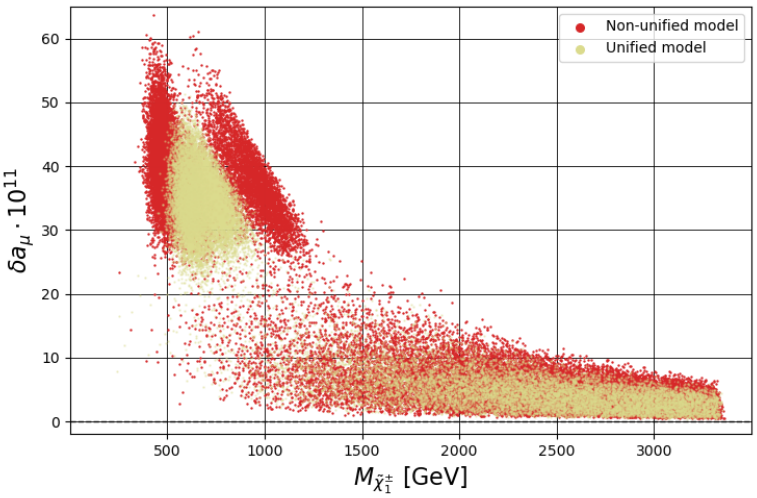

Figure 5.8: The dependence of δa_μ on the first chargino mass in GeV in the unified (yellow) and non-unified (red) model for all runs.

the second run was done with a normal distribution around multiple points with higher δa_μ contributions, the resulting spectra are also expected to have similar masses for charginos and similar contributions. The normal distribution also determines how close the generated points are to the used seeds of the second run. In the previous plots the seed masses were close enough to make the generated model points form one big group, while with the chargino the seeds had a bigger difference in mass between seeds. Therefore the generated points will emerge around the seeds and form multiple groups. The same clustering can be seen in figure (5.3). The overall trend does stay the same as for the slepton and sneutrino, in the sense that we can see that the non-unified model has lighter first chargino solutions and bigger contributions to δa_μ. The fact that the two groups do indeed follow the same trend as seen before in the slepton and sneutrino plots is better represented in figure (5.9), where the two groups are compressed together due to the logarithmic scale on the y-axis. When comparing the plots with each other the same shape can be seen.

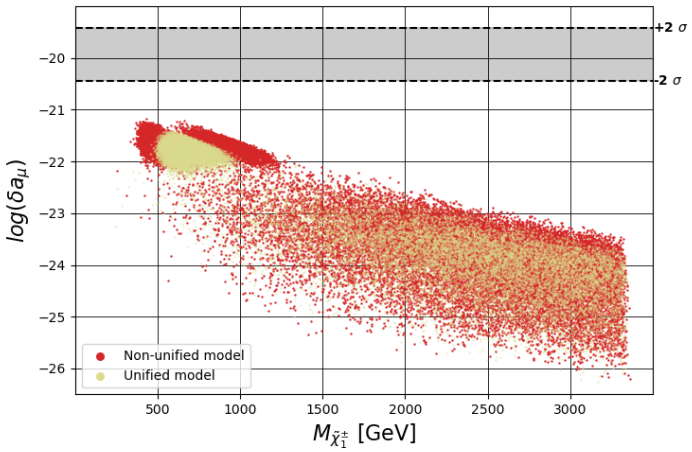

Figure 5.9: The dependence of the logarithm of δa_μ on the first chargino mass in GeV in the unified (yellow) and non-unified (red) model for all runs.

Neutralino mass

The last sparticle to consider is the first neutralino, which is the lightest sparticle. We thus expect the mass of the neutralino to be lighter than the other three sparticle masses. This can be seen in figures (5.10) and (5.11). Simply looking at the scale of the x-axis already shows us that the mass of the first neutralino is in general lower compared to the other sparticles. The unified model seems to reach a minimal first neutralino mass value of 250 GeV, while the non-unified model has lower-mass solutions. These lower masses can have higher contributions to the anomalous magnetic moment than with the unified model. Apart from this feature the graph does not show anything significantly different than what we have discussed before. This is to be expected since the neutralino, apart from being the lightest sparticle, does not have any properties particularly different compared to other sparticles.

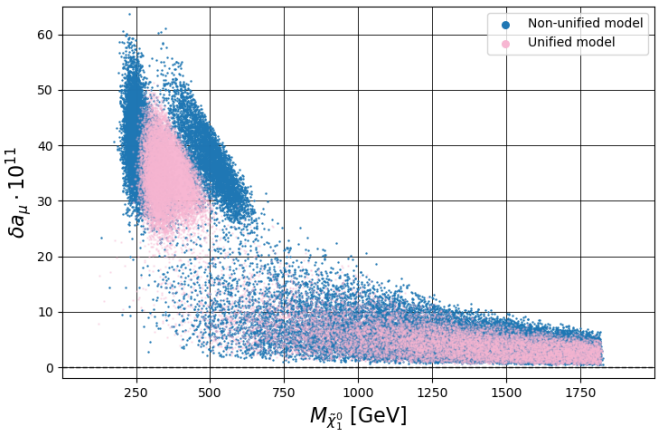

Figure 5.10: The dependence of δa_μ on the first neutralino mass in GeV in the unified (pink) and non-unified (blue) model for all runs.

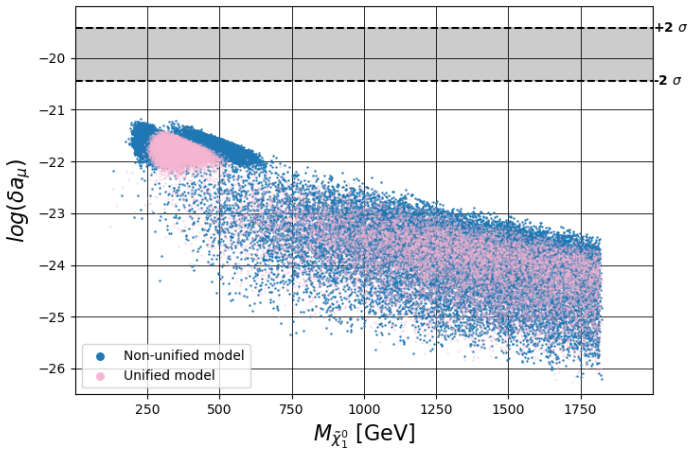

Figure 5.11: The dependence of the logarithm of δa_μ on the first neutralino mass in GeV in the unified (pink) and non-unified (blue) model for all runs.

Other relations

There are many other relations that can cause small contributions to the anomalous magnetic moment, such as the strength of the vertex couplings or the composition of the sparticles. In this thesis we have only looked at the relations between the sparticle mass and δa_μ, but it is still interesting to plot a couple of other relations to see what type of trends we can notice in those plots. The impact of these parameters and their relation to δa_μ is beyond the scope of this thesis, and hence we will refrain from commenting on them. We will show two plots each, normal and logarithmic, for the $\tan(\beta)$ parameter, the trilinear coupling A_0 and some others in Appendix A.

Conclusion

We have discussed some of the effects of SUSY on the muon anomalous magnetic moment using the unified MSSM and the non-unified MSSM. The unified model uses mSUGRA to break the symmetry, while the non-unified model uses a split SUGRA model with m_0 split into left-handed and right-handed terms. In this thesis we have shown how contributions arising from both SUSY models could increase the theoretical value of the muon anomalous magnetic moment. The unified model that we studied was not able to explain the deviation between the theoretical and experimental value of g-2 in a satisfactory manner. Even though the non-unified model showed some model points with a higher a_μ, these were not high enough to explain the deviation between theoretical prediction and experimental values.

During both the first and the second run it proved to be difficult to maintain a correct mass for the Higgs boson. The unified model has to have a high m_0 value to get the correct Higgs boson mass, which was the reason we split the m_0 into two terms. The left-handed m_{0L} was able to decrease in value because the right-handed m_{0R} compensated for this. This subsequently meant that the sparticles, especially the sneutrino, were able to decrease in mass and create higher contributions to a_μ. Further decreases in m_{0L} could create model points that have better contributions, but this would then make it increasingly difficult to maintain the Higgs boson mass. We could use other models outside of SUGRA to break the supersymmetry, but they would also create other limitations that decrease the contribution to a_μ.

There is still a lot to discover and research when it comes to the field of SUSY and in future research looking further into SUGRA could prove to be effective when computing the contribution to the anomalous magnetic moment. In this thesis the analysis and scans of the parameter space are not comprehensive due to time and simplicity constraints. The MSSM model has a total of 105 parameters, while we only used five parameters that then in turn generate many others via the high-scale to low-scale running. For this thesis we have relaxed the constraint of m_0, but this could be done even more in future research: m_0 could be relaxed even more by splitting it for squarks and sleptons. If the program would take higher-order corrections to the Higgs mass into account it would become even more difficult to find good model points that have a high contribution to a_μ. Higher-order Feynman diagrams for supersymmetric particles could also increase the contribution to the anomalous magnetic moment, but these contributions tend to be substantially lower than for the one-loop SUSY Feynman diagrams.

In this thesis we have shown that SUSY, specifically the non-unified MSSM model, does not explain the deviation between theoretical and experimental values sufficiently. In 2024 the J-PARC centre in Japan will conduct new research increasing the accuracy of the experimental value, likewise the theoretical uncertainty will also keep decreasing as more numerical corrections for higher orders get computed. If the experimental value stays the same while the error decreases, the deviation will become significant enough to call for new physics. Even though the models in this thesis did not explain the g-2 discrepancy sufficiently, we have shown that the non-unified model can better contribute to the muon anomalous magnetic moment than the unified model.

Bibliography

[1] John D. Jackson. "5.6: Magnetic fields of a Localized Current Distribution, Magnetic Moment". *Classical Electrodynamics*, pp: 145–148, 1962.

[2] Michael E. McHenry and David E. Laughlin. "Magnetic moment and magnetization". *Characterization of Materials*, p: 2, 2012.

[3] David J. Griffiths. "6: Magnetic Fields in Matter". *Introduction to Electrodynamics*, pp: 266–296, 1981 , 4th edition.

[4] MikeRun. "Electron orbital magnetic moment", 2020. https://commons.wikimedia.org/wiki/File:Electron-orbital-magnetic-moment.svg.

[5] Stan Zurek. "Torque on magnetic dipole magnetica", 2020. https://e-magnetica.pl/file/torque_on_magnetic_dipole_magnetica_png.

[6] Brian H. Bransden and Charles J. Joachain. "Appendices 7: The Dirac equation and relativistic corrections to the Schrödinger equation". *Physics of atoms and molecules*, pp: 631–641, 1983.

[7] Simon Eidelman and Massimo Passera. "Theory of the τ lepton anomalous magnetic moment". *Modern Physics Letters A*, pp: 159–179, 2007.

[8] Tareq A. Albahri et al. (Muon g 2 Collaboration). "Measurement of the anomalous precession frequency of the muon in the Fermilab Muon g - 2 experiment". *Phys. Rev. D 103, 072002*, pp: 1–29, 2021.

[9] Babak Abi et al. (Muon g 2 Collaboration). "Measurement of the Positive Muon Anomalous Magnetic Moment to 0.46 ppm". *Phys. Rev. Lett. 126, 141801*, pp: 1–11, 2021.

[10] Tatsumi Aoyama et al. "The anomalous magnetic moment of the muon in the Standard Model". *Phys. Rept. 887*, pp: 1–179, 2020.

[11] Eremey Valetov (Fermilab). "The Muon g–2 Experiment", 2019. https://lss.fnal.gov/archive/2019/slides/fermilab-slides-19-091-e.pdf.

[12] Fermilab PBS NOVA. "Standard Model of Elementary Particles", 2019. https://en.wikipedia.org/wiki/File:Standard_Model_of_Elementary_Particles.svg.

[13] Piotr A. Zyla et al. (Particle Data Group). "Review of Particle Physics". *Prog. Theor. Exp. Phys. 2020, 083C01*, pp: 722–725, 2020.

[14] Michael E. Peskin and Daniel V. Schroeder. "6.3: The Electron Vertex Function: Evaluation". *An Introduction to Quantum Field Theory*, pp: 189–196, 1995.

[15] Toichiro Kinoshita et al. "Eighth order QED contribution to the anomalous magnetic moment of the muon". *Phys. Rev. D 41, 593*, pp: 1–18, 1990.

[16] Tatsumi Aoyama et al. "Complete Tenth-Order QED Contribution to the Muon g-2". *Phys. Rev. Lett. 109, 111808*, pp: 1–4, 2012.

[17] Fred Jegerlehner and Andreas Nyffeler. "The Muon g-2". *Phys. Rept. 477, 1*, pp: 80–94, 2009.

[18] Shu-Min Zhao et al. "Study muon g - 2 at two-loop level in the U(1)XSSM". *Journal of High Energy Physics 2022, 3*, pp: 1–31, 2022.

[19] Ben Allanach. "Beyond the Standard Model". *CERN Yellow Reports: School Proceedings, 5 Geneva*, p: 5, 2017.

[20] Hitoshi Murayama. "Supersymmetry phenomenology". *Lawrence Berkeley National Laboratory*, pp: 1–40, 2000.

[21] Ali H. Chamseddine et al. "Locally Supersymmetric Grand Unification". *Phys. Rev. Lett. 49, 970*, pp: 1–40, 1982.

[22] Steven Weinberg. "6.2: Calculation of the Propagator". *The Quantum Theory of Fields, volume I Foundations*, pp: 274–280, 1995.

[23] Dominik Stöckinger et al. "Photonic SUSY Two-Loop Corrections to the Muon Magnetic Moment". *Phys.Rev.D81:093004*, pp: 1–25, 2010.

[24] Florian Staub. "SARAH". *Hepforge*, pp: 1–153, 2012.

[25] Florian Staub and Werner Porod. "SPheno 3.1: extensions including flavour, CP-phases and models beyond the MSSM". *Computer Physics Communications 183*, pp: 1–17, 2011.

A Appendix

In this appendix a couple of graphs are placed that show the relation between different parameters and δa_μ.

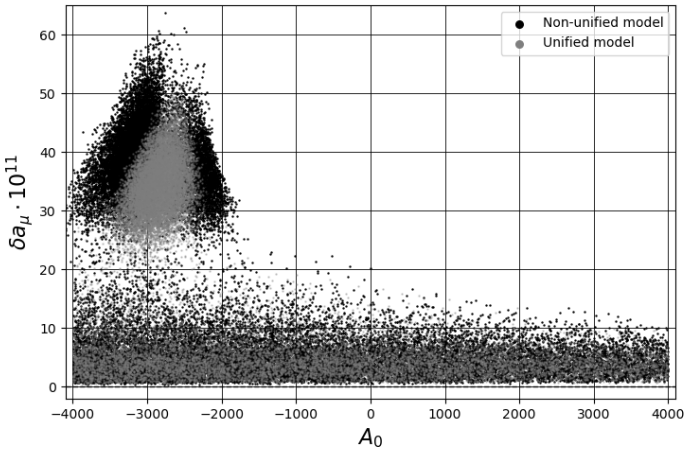

Figure A.1: The dependence of δa_μ on the trilinear coupling in GeV in the unified (grey) and non-unified (black) model for all runs.

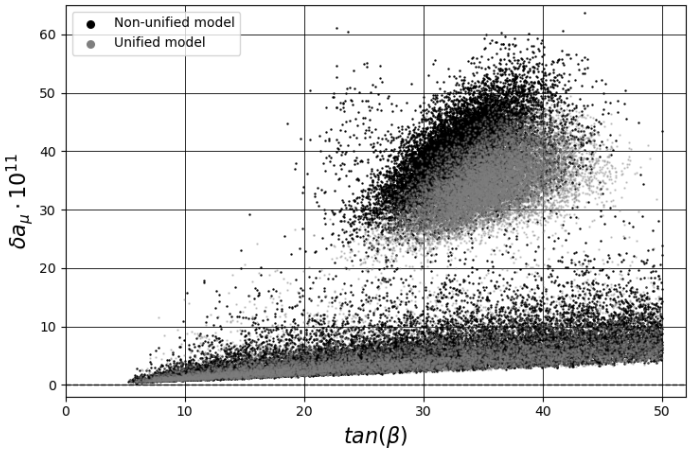

Figure A.2: The dependence of δa_μ on $tan(\beta)$ in the unified (grey) and non-unified (black) model for all runs.

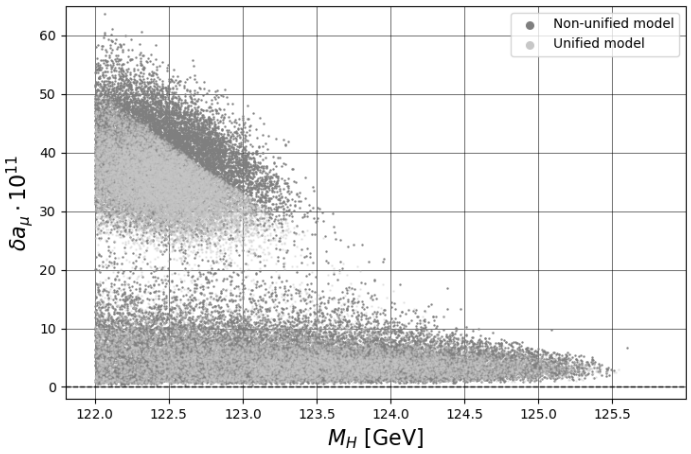

Figure A.3: The dependence of δa_μ on the Higgs mass in GeV in the unified (grey) and non-unified (dark grey) model for all runs.

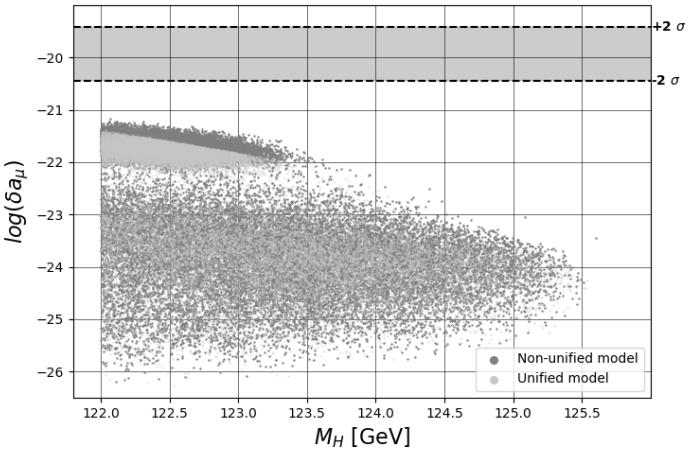

Figure A.4: The dependence of the logarithm of δa_μ on the Higgs mass in GeV in the unified (grey) and non-unified (dark grey) model for all runs.